Journal of Catalysis 269 (2010) 33–43

Contents lists available at ScienceDirect

Journal of Catalysis

journal homepage: www.elsevier.com/locate/jcat

Selective decomposition of formic acid on molybdenum carbide: A new reaction pathway

David W. Flaherty, Sean P. Berglund, C. Buddie Mullins *

Department of Chemical Engineering, Texas Materials Institute, Center for Nano- and Molecular Science and Technology, Center for Electrochemistry, 1 University Station, CO400, University of Texas at Austin, Austin, TX 78712, United States

ARTICLE INFO

Article history:
Received 31 August 2009
Revised 13 October 2009
Accepted 15 October 2009
Available online 12 November 2009

Keywords:
Transition metal carbide
Selective dehydrogenation
Infrared spectroscopy
Carboxyl
Formate

ABSTRACT

Selective decomposition of formic acid is important as a prototype to study selective bond cleavage of oxygenates. We demonstrate that carbon-modified Mo(1 1 0), C–Mo(1 1 0), is up to 15 times more selective for the dehydrogenation of formic acid than Mo(1 1 0). Reflection absorption infrared spectroscopy (RAIRS) indicates that carbidic carbon blocks active sites for C–O bond cleavage, decreasing the rate of dehydration. Steady-state reactive molecular beam scattering (RMBS) shows that dehydration is the dominant reaction pathway on clean Mo(1 1 0), while C–Mo(1 1 0) selectively promotes dehydrogenation. Kinetic analysis of RMBS data reveals that formic acid dehydrogenation on Mo(1 1 0) has an activation energy of 34.4 ± 3.3 kJ mol^{-1} while the C–Mo(1 1 0) surface promotes distinct pathways for dehydrogenation with an activation energy of only 12.8 ± 1.0 kJ mol^{-1}. RAIRS spectra suggest the new pathways include the formation of monodentate formate, and at temperatures of 500 K and greater, direct activation of the C–H bond to form carboxyl, both of which decompose via a $CO_2^{\delta-}$ intermediate to evolve CO_2 and H_2.

1. Introduction

Transition metal carbides (TMCs) have attracted significant interest following seminal research by Boudart and co-workers who reported platinum-like reactivity of tungsten carbide catalysts [1]. Since this discovery numerous research groups have investigated the reactivity of transition metal carbides with particular focus on Group VI TMCs, namely tungsten and molybdenum carbides [2–4]. Early transition metals have high binding energies for many molecules preventing facile desorption and repeated reaction. However, their catalytic behavior can be improved by tempering the binding energy of adsorbates through the addition of carbon and subsequent carbide formation. Many investigations have shown that TMCs can catalyze a number of reactions (many at rates matching or exceeding the best known Group VIII transition metals) involving hydrogen transfer (hydrogenation, isomerization, hydrodesulfurization) [5]. Molybdenum carbide (Mo_2C) in particular has been shown to be active for hydrogenation and dehydrogenation reactions [6], and recent research has demonstrated that Mo_2C is highly active for the low temperature water–gas shift reaction, in some cases performing better than commercial alumina supported Cu–Zn catalysts [7–11]. Further, TMCs have the added benefits of comparatively low cost (with respect to Pt-group metals), high thermal stability, mechanical durability, and greater tolerance to common catalyst poisons [2,6]. In addition to the immediate economic benefits of using TMCs as replacements for precious metal catalysts, it is necessary to consider the sustainability of relying on such rare materials. The US Geological Survey estimates the relative abundance[1] of Pd, Pt, Rh and Ir as 7×10^{-4}, 7×10^{-4}, 2×10^{-4}, and 1×10^{-5} [12]. In sharp contrast Mo and W (two of the metals used for TMC catalysts) have a relative abundance[1] of 2 and 1, making them $\sim 10^3$–10^5 times more abundant than the Pt-group elements.

Significant demand for platinum and platinum-based alloy catalysts has been generated by the need for oxygen reduction and fuel oxidation catalysts for fuel cells. The ubiquitous proton exchange membrane fuel cell (PEMFC) suffers from well known disadvantages due to the use of hydrogen fuel (storage costs and safety) which has promoted interest in alternative liquid fuel cells. Direct Formic Acid Fuel Cells (DFAFCs) are a safe and convenient alternative for portable applications [13–15]. Still, DFAFCs utilize Pt and Pd-based catalysts; in fact, the most active reported

* Corresponding author. Fax: +1 512 471 7060.
E-mail address: mullins@che.utexas.edu (C.B. Mullins).

[1] Relative abundance of each element is expressed as atoms of the element per 10^6 atoms of Si in the earth's upper crust.

0021-9517/$ - see front matter © 2009 Elsevier Inc. All rights reserved.
doi:10.1016/j.jcat.2009.10.012

catalysts are Pd–Pt alloys [15–17]. Electrochemical investigations have established that CO formed by HCOOH decomposition acts to poison active sites, gradually deceasing the activity of the catalyst [18]. Whereas removal of CO can be achieved by oxidation to CO_2 by reaction with adsorbed hydroxyl groups present on the surface, in a manner somewhat analogous to the associative water–gas shift mechanism, this reaction appears to be slow and consequently in some cases is a rate-limiting step [18]. The greater activity of Pd-based electrocatalysts has been attributed to an increased rate for direct conversion of formic acid to CO_2 which avoids the formation of CO [15,16]. Therefore, a potential catalyst for formic acid decomposition should promote direct dehydrogenation of formic acid with high activity for CO removal by desorption or by oxidation with surface hydroxyls. The catalytic behavior of formic acid with Mo_2C has not been investigated, although Mo_2C and WC have already shown promise as replacements for platinum anodes in PEMFCs [19] and direct methanol fuel cells [20].

In many cases, especially for energy applications, the overall desired reaction is dehydrogenation [$HCOOH \rightarrow CO_2 + H_2$][2] as opposed to dehydration [$HCOOH \rightarrow CO + H_2O$]. Thus, it is of primary interest to determine the elementary steps of the reaction pathway and how these steps may be influenced or controlled by careful modification of the catalyst. The surface chemistry of formic acid has been reviewed by Columbia and Thiel [21], although a number of investigations have been performed since. Briefly, on many clean and oxygen modified transition metal surfaces formic acid initially reacts to create formate and other surface species by either (a) unimolecular deprotonation [$HCOOH \rightarrow HCOO + H$] or (b) bimolecular dehydration [$2HCOOH \rightarrow HCOO + H + HCO + OH$]. After this first step, the formate species undergoes one of the following reactions; (c) unimolecular deprotonation [$HCOO \rightarrow CO_2 + H$], (d) reaction with a second formate molecule through the bimolecular "hot hydrogen" pathway [$2HCOO \rightarrow CO + CO_2 + 2H + O$], or (e) complete decomposition to atomic surface species. In all cases, the ultimate fate of the products from these reaction mechanisms is strongly influenced by the binding energy of these species to the surface, dictating whether they undergo direct desorption, recombinative desorption, or complete dissociation. In the case of Group VIII transition metals, ultra-high vacuum (UHV) studies show that formic acid adsorption on to the clean metal surfaces followed by temperature programmed desorption reacts both by dehydrogenation and dehydration to yield comparable amounts of CO_2 and CO on Ni(1 0 0) [22], Ni(1 1 0) [23,24], Ni(1 1 1) [25], Ru(0 0 0 1) [26], Pd(1 1 1) [27,28] and Pt(1 1 0) [29]. On the other hand, only CO_2 and H_2 evolve from the reaction of formic acid dosed at low temperatures on Pt(1 1 1) [30,31], while the Pt(1 0 0) surface is reported to be inert to formic acid [32]. Additionally, Dahlberg et al. investigated the steady-state reaction of formic acid on polycrystalline platinum foil by molecular beam and found that the reaction proceeded with ~85% selectivity towards dehydrogenation [33].

Here, we investigate the reaction of formic acid on molybdenum and molybdenum carbide surfaces using two general approaches. First, formic acid decomposition was studied using reflection absorption infrared spectroscopy (RAIRS) and temperature programmed desorption (TPD) on a clean molybdenum surface, Mo(1 1 0), and a molybdenum carbide model catalyst, C–Mo(1 1 0) to determine the effects of carburization towards selective bond cleavage. Vibrational spectroscopy performed in this study indicates that the addition of carbon suppresses low temperature C–O bond dissociation on C–Mo(1 1 0) in comparison to Mo(1 1 0), creating less CO during the initial stages of formic acid decomposition. Second, formic acid decomposition was investigated utilizing reactive molecular beam scattering (RMBS) on the two model catalysts, Mo(1 1 0) and C–Mo(1 1 0). Analysis of the kinetics of this reaction at near steady-state conditions, in a manner comparable to the investigation of Dahlberg et al. on Pt [33], provides product selectivities and apparent activation energies for the direct dehydrogenation and dehydration reaction pathways for formic acid decomposition. Results from these "single-collision" experiments demonstrate that carburization of the Mo(1 1 0) surface improves selectivity towards direct gas phase dehydrogenation at steady-state by as much as ~1500%. Kinetic data and vibrational spectra acquired at steady-state suggest that the increased selectivity is due to two individual effects: (1) carbidic carbon decreases the rate of dehydration without modifying the activation energy, which remains nearly constant at ~16 kJ mol^{-1}, therefore, it seems that carbon atoms block the active sites responsible for dehydration, and (2) formation of a carbidic layer on Mo(1 1 0) decreases the apparent activation energy for dehydrogenation from 34.4 ± 3.3 to 12.8 ± 1.0 kJ mol^{-1} suggesting a change in the reaction mechanism due to the presence of carbidic carbon. Vibrational spectroscopy indicates that carbon-modified Mo(1 1 0) generates new, distinct surface intermediates which are absent on unmodified Mo(1 1 0) including monodentate formate, anionic carbon dioxide, $CO_2^{\delta-}$, and carboxyl, OCOH.

2. Experimental

Our experiments investigating the reaction of formic acid with molybdenum carbide were conducted employing an ultra-high vacuum (UHV) molecular beam surface scattering apparatus with a base pressure less than 1×10^{-10} Torr which has been previously described in detail [34]. Briefly, the apparatus contains an Auger electron spectrometer (AES, Physical Electronics 10–500), a quadrupole mass spectrometer (QMS, Extrel C-50), a Fourier transform infrared spectrometer (FTIR, Bruker Tensor 27) combined with a mercury–cadmium–telluride detector (MCT, Infrared Associates) for reflection absorption infrared spectroscopy (RAIRS), as well as nozzles and apertures for generating two separate molecular beams which are used in combination with the QMS to conduct temperature programmed desorption (TPD) and reactive molecular beam scattering (RMBS) experiments. Additionally, the chamber contains electron beam evaporators (Omicron, EFM3) and a quartz crystal microbalance (QCM, Maxtek) for thin film deposition and an Ar ion sputter gun (Ar^+, RBD Enterprises) for sample cleaning. The Mo(1 1 0) single crystal (Surface Preparation Lab, 10 mm × 10 mm × 1.5 mm) is spot-welded to adjacent 1 mm molybdenum posts and mounted on a liquid nitrogen cooled probe. The sample temperature is measured with a type-C thermocouple spot-welded to the backside of the sample and controlled by resistive heating over the range 77–1850 K. The absolute temperature (±2 K) is verified using the known multilayer desorption temperatures of several small molecules. The clean Mo(1 1 0) surface is prepared by alternating cycles of high temperature annealing in oxygen (1200 K, 5×10^{-7} Torr) and Ar ion sputtering. Several cycles were typically required to remove all carbon and oxygen contamination from the surface. The clean surface is estimated to have less than 2% residual carbon and oxygen contamination as estimated by AES.

The Mo_2C model catalyst was generated using the approach of Frühberger and Chen [35,36]. Briefly, the Mo(1 1 0) sample is exposed to 15 Langmuirs (1 L = 1×10^{-6} Torr s) of ethylene at 600 K and subsequently heated to 1200 K. This treatment is typically repeated three times followed by annealing at 1200–1400 K which allows accumulated carbon to diffuse into the sample. Characterization utilizing low energy electron diffraction (LEED), AES, and near-edge X-ray absorption fine structure (NEXAFS) has indicated

[2] In electrochemical systems this reaction is more accurately expressed as $HCOOH \rightarrow CO_2 + 2H^+ + 2e^-$.

that this sample preparation technique creates a thin epitaxial layer resembling carbon-terminated Mo_2C on Mo(1 1 0) [4,36,37]. After repeated exposure to ethylene and annealing, AES indicates that the sample surface region (topmost 5–10 atomic layers) has an overall carbon to molybdenum atomic ratio of 0.39–0.45. Throughout this paper, the thin film Mo_2C model catalyst supported on Mo(1 1 0) created in this manner will be referred to as C–Mo(1 1 0). In addition to AES, infrared spectroscopy of CO adsorbed at 77 K was utilized to monitor the stoichiometry and cleanliness of the surface. Prior to each experiment, RAIRS of CO adsorbed on the sample was utilized to confirm the carbidic or metallic state of the surface and its homogeneity. McBreen and co-workers observed ν(CO) at 2057–2072 cm^{-1} from CO adsorbed at on-top sites on polycrystalline β-Mo_2C foils [38]. In agreement with previous work, a saturation coverage of CO on Mo(1 1 0) creates absorption features at 1895 and 2039 cm^{-1} due to adsorption at long-bridge and on-top sites [39,40]. Alternatively, CO adsorption on C-Mo(1 1 0) at 77 K leads to a single vibrational peak at 2089 cm^{-1} due to adsorption at on-top sites [40].

Infrared spectra of formic acid and the subsequent surface intermediates were collected by reflection absorption infrared spectroscopy (RAIRS) by adsorption of 2 ML of HCOOH (Acros, 98+%) or DCOOH (Cambridge Isotope, 98+%) at 77 K, followed by incremental heating to the indicated temperature for each spectrum, and rapid cooling to 77 K before collecting each spectrum, except in the case of RMBS experiments. For vibrational spectroscopy of surface intermediates formed during RMBS experiments, the sample and background RAIRS spectra were both acquired at the indicated experimental temperature. Acquisition of the infrared spectrum was started after the RMBS experiment reached near steady state conditions, as indicated by a constant partial pressure of each product with respect to time. Each RAIRS experiment was repeated three times, to judge reproducibility and to increase the signal-to-noise ratio. The scans were co-added for a total of 3072 scans at 4 cm^{-1} resolution. Temperature programmed desorption (TPD) experiments were conducted by adsorbing HCOOH at 77 K via molecular beam followed by heating to 1200 K at 4 K s^{-1}. The quadrupole mass spectrometer was utilized to determine desorption products by monitoring the following m/z^+ ratios for each product: HCOOH (46, 44, 29, 28), CO_2 (44, 28), H_2 (2), CO (28), H_2O (18). Additionally, the formation of formaldehyde was ruled out by monitoring m/z^+ 30 and 29 simultaneously with the previous masses. Reactive molecular beam scattering (RMBS) experiments were conducted by impinging a molecular beam of HCOOH molecules with known flux ($\sim 1.4 \times 10^{15}$ molecules cm^{-2} s^{-1}) onto the sample surface at a selected temperature (350–700 K). The overall rate of reaction was determined by using an inert stainless steel flag to establish a baseline by which to compare the reactive surfaces. The QMS was utilized, as described for TPD measurements, to identify and quantify the reaction products and the overall rate of HCOOH decomposition. Absolute quantities of the reaction products (CO_2, H_2, CO, and H_2O) were calculated by calibrating the QMS response for each molecule using two independent methods which agreed within ~30%. The first method involved accounting for the pumping speed of each molecule in the vacuum chamber; the fragmentation pattern of each molecule due to electron impact and ionization; and the mass spectrometer sensitivity towards individual ionic species. The relative ionization probability for each species was accounted for using a nude ion gauge to calculate the QMS response (counts·s^{-1} per Torr). The second method utilized the adsorption of small quantities of formic acid onto the C–Mo(1 1 0) sample. Analysis of the products (only CO and H_2 for the conditions used) yielded the correction factors for the QMS sensitivity towards these two species only. A detailed description of these techniques can be found in the Supplementary material.

3. Results and discussion

3.1. Infrared spectroscopy of HCOOH and DCOOH

Infrared spectra of HCOOH and DCOOH adsorbed onto the Mo(1 1 0) surface are displayed in Fig. 1a and b while spectra on the C–Mo(1 1 0) surface are displayed in Fig. 2a and b. At a sample temperature of 77 K formic acid remains intact on both surfaces (i.e., Mo(1 1 0) and C–Mo(1 1 0)) and the vibrational spectra closely resemble each other and published spectra of crystalline HCOOH and HCOOH multilayers on Mo(1 1 0) [41,42]. The distinct absorption peaks corresponding to fundamental vibrational modes of HCOOH (Fig. 1a) are evident at 714, 963, 1078, 1237, 1388, 1737, and 2943 cm^{-1} which correspond to the δ(OCO), π(OH), π(CH), ν(C–O), δ(CH), ν(C=O) and ν(CH) normal modes, respectively. There is also a broad absorption feature which occurs between 2900–3050 cm^{-1} which is assigned to the ν(OH) mode of formic acid molecules within hydrogen bonded chains on the surface [21,43–45]. Additionally, two broad peaks are apparent at 2584 and 2758 cm^{-1} which are attributed to the combination features of ν(C=O) + π(OH) and ν(C=O) + π(CH), respectively, as identified by Mikawa et al. [41]. To minimize ambiguity in peak assignments identical experiments were conducted utilizing DCOOH on Mo(1 1 0) and these RAIRS spectra are shown in Fig. 1b. Primary isotope shifts due to the substitution of deuterium for hydrogen (DCOOH instead of HCOOH) are frequently observed to decrease the primary normal mode frequencies by a factor of $\sim\sqrt{2}$ allowing

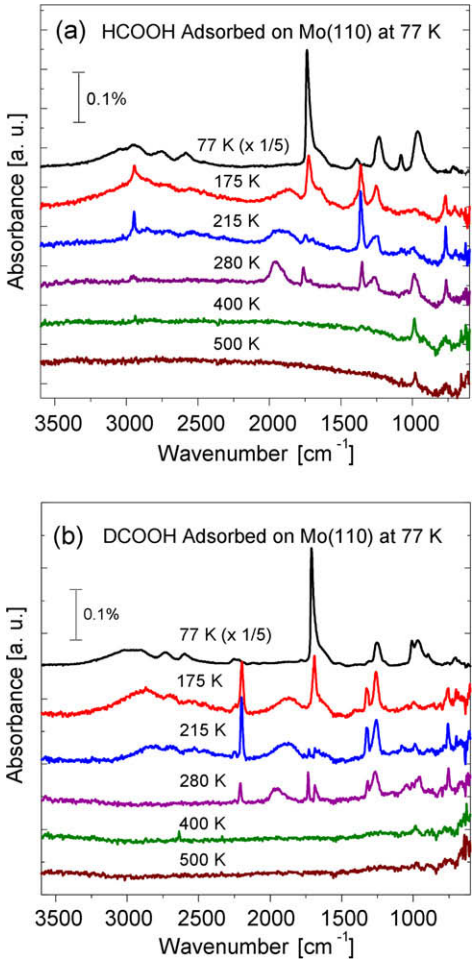

Fig. 1. RAIRS spectra of (a) HCOOH and (b) DCOOH adsorbed on Mo(1 1 0). Formic acid is adsorbed at 77 K via molecular beam followed by incremental heating to each temperature. The sample is cooled to 77 K before collecting each spectrum.

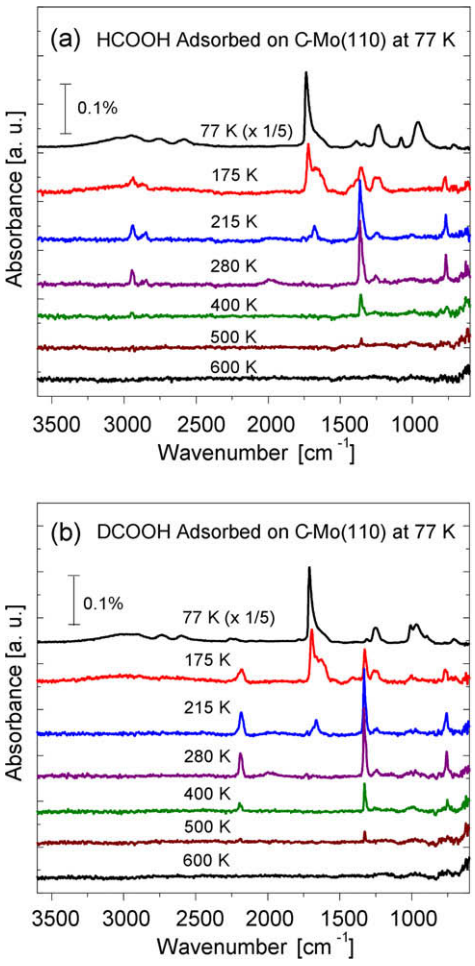

Fig. 2. RAIRS spectra of (a) HCOOH and (b) DCOOH adsorbed on C–Mo(1 1 0). Formic acid is adsorbed at 77 K via molecular beam followed by incremental heating to each temperature. The sample is cooled to 77 K before collecting each spectrum.

for more certainty in peak identification. In this case, vibrational peaks which should decrease by a factor of $\sim\sqrt{2}$ and therefore directly involve the isotope are those attributed to the ν(C–H/D), δ(C–H/D), and π(C–H/D) vibrational modes as well as combinations involving these. The peak assignments for both HCOOH and DCOOH are summarized in Table 1.

As the samples are heated, infrared spectroscopy reveals key information about the reaction pathway and adsorbate geometry on the Mo(1 1 0) surface. Heating to temperatures greater than 160 K leads to desorption of the formic acid multilayer, as demonstrated via TPD measurements (shown later), thus heating to 175 K greatly reduced the intensity of the associated vibrations [30,42]. Even at 175 K, a significant fraction of the remaining formic acid reacts on Mo(1 1 0). New absorption features evolve at 767, 1267, 1353, 1746, and 2949 cm^{-1} which are assigned to two distinct formate species, as discussed below. In addition, a broad feature develops at 1870 cm^{-1} which Goodman and co-workers have identified as formyl, specifically the ν(CO) mode of the HCO species [42]. Molecular formic acid remains on the surface up to ~280 K. The presence of both formate and formyl at 175 K indicates that both O–H and C–O bonds are broken, which is consistent with initial dissociation proceeding via a bimolecular dehydration reaction as discussed by Columbia and Thiel [21]. Infrared spectra do not show the presence of water or hydroxyl groups on the surface at 175 K; however, there are several reasons that this may be. First, the ν(OH) stretch for water may overlap with the remaining ν(OH) modes of formic acid and be indistinguishable. Additionally, molecular water on Mo(1 1 0) generally desorbs at low temperatures ($T < 200$ K) or is dissociated over the temperature range 140–230 K [46]. Then most likely, only small amounts of water will evolve from the surface due to the recombination of OH and H. These intermediates may prefer to recombinatively desorb as H_2 at ~350 K leaving atomic oxygen on the surface [46].

Heating from 175 to 215 K and then further to 280 K clearly illustrates the decomposition and desorption of the remaining formic acid as determined by the disappearance of the carbonyl stretching mode, ν(C=O), at 1737 cm^{-1}. Simultaneously, the amount of formate reaches a maximum at 215 K and then diminishes slightly by 280 K as seen by the changes of intensity of features at 767, 1273, 1353, and 1746 cm^{-1}. Formyl also decomposes within this temperature range to adsorbed CO and atomic hydrogen as suggested by the shift of $\nu(CO)_{HCO}$ at 1870 cm^{-1} to $\nu(CO)_{CO}$ at 1960 cm^{-1} at 280 K. Xu et al. observed overlapping features at ~980 cm^{-1} which were attributed to ν(Mo–O) and ν(Mo–H) [42]. However, other investigators have reported ν(Mo–H) at higher wavenumbers such as on Mo(1 0 0) at 1030–1260 cm^{-1} and on Mo(1 1 0) at 1096–1226 cm^{-1} [47,48]. In this study, a very small peak is apparent at ~1070 cm^{-1} which corresponds to ν(Mo–H) from hydrogen atoms adsorbed at pseudo threefold hollow sites on the Mo(1 1 0) surface [48]. Following adsorption of DCOOH, this feature is still observed at 1070 cm^{-1} demonstrating that atomic hydrogen originates from the hydroxyl group of formic acid. Additionally, this feature disappears at temperatures greater than 400 K which correlates to H_2 evolution observed in TPD experiments. A stronger vibrational peak located at 986 cm^{-1} closely matches the on-top atomic oxygen species observed on Mo(1 1 0) by Colaianni et al. [39] and Queeney and Friend [49]. On-top oxygen has only been observed for high oxygen coverages on Mo(1 1 0), generally oxygen atoms prefer to bind at higher coordination sites such as the pseudo threefold hollow and long-bridge sites [39]. In this case, on-top ν(Mo–O) could result from the dissociation of hydroxyl groups formed by dehydration (HCOOH → HCO + OH) following the occupation of higher coordination sites by other surface species, such as CO.

Table 1
Normal mode assignments for HCOOH and DCOOH.

Mode	Crystalline HCOOH [41]	HCOOH Mo(1 1 0) [42]	HCOOH [DCOOH] Mo(1 1 0)	HCOOH [DCOOH] C–Mo(1 1 0)
νCH	2960	2960	2948 [2253]	2943 [2258]
νOH	2900	–	3050–2900 [3025–2900]	3050–2900 [3020–2900]
νC=O + πCH	2700	–	2758 [2733]	2753 [2734]
νC=O + πOH	2540	–	2584 [2600]	2584 [2595]
νC=O	1620	1720	1737 [1712]	1737 [1711]
δCH	1370	1400	1388 [1009]	1388 [1008]
νC–O	1248	1230	1233 [1253]	1237 [1253]
πCH	1078	1070	1078 [896]	1078 [895]
πOH	947	950	963 [968]	963 [969]
δOCO	720	700	714 [704]	714 [712]

The geometry of formate on Mo(1 1 0) can be determined by examining the spectrum obtained at 280 K and by considering which vibrational modes are IR active on the surface. Vibrational modes attributed to formate occur at 767, 1273, 1353, 1746, and 2950 cm^{-1} (features at 986 and 1960 cm^{-1} originate from adsorbed CO and atomic hydrogen as previously discussed). Three individual geometries are possible for formate; bridge-bonded (C_{2v} symmetry, oxygen atoms coordinated to separate surface atoms), bidentate (C_{2v} symmetry, oxygen atoms bonded to the same surface atom), and monodentate (C_s symmetry, a single oxygen bound to the surface with the carbonyl free). In this study, the bridge-bonded and bidentate bond configurations are not distinguishable; however, high resolution electron energy loss spectroscopy (HREELS) has been successfully utilized in a non-specular configuration to differentiate between these two geometries [43]. Hence, we will refer only to bridge-bonded formate. For RAIRS measurements only vibrational normal modes with a dipole component perpendicular to the surface are detectable. Consequently, bridge-bonded formate and monodentate formate have different IR active modes which can be used to distinguish the identity of the species present. Fig. S1 in Supplementary material illustrates the active and inactive vibrational modes associated with both the bridge-bonded and monodentate structures.

Briefly, for bridge-bonded formate with the molecular plane normal to the surface, only the δ(OCO), ν_s(OCO), and ν(CH) modes are infrared active due to the internal symmetry of the molecule (which negates the perpendicular contribution of the ν_a(OCO) mode) and surface selection rules (which rule out the detection of any dipoles parallel to the surface). Inspection of the RAIRS spectrum with these selection rules in mind suggests that features at 767, 1353, and 2949 cm^{-1} correspond to the δ(OCO), ν_s(OCO), and ν(CH) vibrational modes of a bridge-bonded formate species. Monodentate formate has lower symmetry; therefore, additional vibrational normal modes are IR active. Peaks at 767, 1267, 1746, and 2949 cm^{-1} correspond closely to δ(OCO), ν_s(OCO), ν_a(OCO) and ν(CH) of monodentate formate. The peak assignments for the individual formate species observed are summarized in Supplementary material (Table S1). These assignments are in close agreement with previous observations of bridge-bonded or bidentate formate on Ru(0 0 0 1) [45], Pt(1 1 1) [30,31], NiO(1 1 1) [50,51], and Ni(1 1 0) [52] as well as assignments of monodentate formate on oxygen modified surfaces including O–Ru(0 0 0 1) [45], O–Pt(1 1 1) [53], NiO(1 1 1) [51], O(2 × 1) Ni(1 1 0) and carbidic C(4 × 5) Ni(1 1 0) [52]. A comparison of the intensity of the ν_s(OCO) modes of monodentate and bridge-bonded formate (1267 and 1353 cm^{-1}, respectively) is ~1:2. Assuming that RAIRS has equal sensitivity for these two vibrational modes, this ratio suggests that the relative ratio of monodentate formate to bridge-bonded formate should also be ~1:2. Later in the paper, this value will be compared to an equivalent analysis performed on the C–Mo(1 1 0) surface. Both formate species decompose as the sample is heated to 400 K as indicated by attenuation of all the associated features. Additionally the ν(CO) feature for CO disappears which is due to the molecular desorption of a fraction of the CO on the surface followed by the dissociation of that which remains at 350 K [54,55]. At temperatures of 400–500 K, the only persisting vibrational feature is that of ν(Mo–O) at 986 cm^{-1} which remains until ~600 K. Oxygen does not desorb from Mo(1 1 0) until temperatures of 1800–2000 K, although recombination of atomic carbon and oxygen occurs at ~1000 K. Therefore the disappearance of ν(Mo–O) is attributed to the migration of atomic oxygen to higher coordination sites. Reported values for the ν_s(Mo–O) modes of atomic oxygen in long-bridge sites and pseudo threefold hollow sites are 545 and 645 cm^{-1}, respectively [39]. Unfortunately, these values lie below the cut-off frequency of the RAIRS system used here, ~700 cm^{-1}, and cannot be directly observed.

Infrared spectra of formic acid multilayers on C–Mo(1 1 0) are very similar to those on Mo(1 1 0) as they are expected to be fairly independent of the substrate. However, subsequent heating reveals that the reaction pathway and resulting surface intermediates display several key differences, as shown in Fig. 2a and b. After heating HCOOH adsorbed on C–Mo(1 1 0) to 215 and 280 K, new absorption features evolve at 768, 1255, 1363, 1759, and 2945 cm^{-1} which are assigned to a combination of monodentate and bridge-bonded formate species, as discussed above for the case of Mo(1 1 0). A new feature is evident at 2851 cm^{-1} for HCOOH adsorption on C–Mo(1 1 0), which is ascribed to a combination of the ν_a(OCO) + δ(CH) modes through dipole interactions which concomitantly experience Fermi resonance leading to a downward shift of the ν(CH) normal mode [56]. Other vibrational features indicate that the geometry of the formate species on C–Mo(1 1 0) is modified from Mo(1 1 0). Whereas formic acid adsorption and heating resulted in a 1:2 ratio of monodentate to bridge-bonded formate on Mo(1 1 0) upon heating to 280 K, C–Mo(1 1 0) produces a distinctly smaller amount of monodentate in comparison to bridge-bonded formate, a ratio of about 1:10. Furthermore, spectra of both HCOOH and DCOOH on C–Mo(1 1 0) at 280 K reveal that the $\nu(CO)_{CO}$ feature is greatly attenuated. On Mo(1 1 0) at 280 K, the intensity of the $\nu(CO)_{CO}$ feature was ~60–70% of that of the formate ν_s(OCO) feature; however, on C–Mo(1 1 0) the intensity is diminished to ~10%. This directly demonstrates that significantly less formyl, and eventually CO, is produced on C–Mo(1 1 0) indicating that carbon modification of Mo(1 1 0) greatly reduces the extent of low temperature ($T < 280$ K) C–O bond cleavage, a necessary step for dehydration. Additionally, the ν(Mo–O) feature is absent from vibrational spectra acquired on C–Mo(1 1 0). This does not necessarily mean that atomic oxygen is not present on the surface (oxygen atoms in higher coordination sites would be observed at frequencies less than 700 cm^{-1}, as stated before), however the lack of on-top oxygen atoms does suggest that the overall amount of decomposition is decreased. Greater amounts of bridge-bonded formate present on the surface may be directly linked to the decreased production of formyl. These observations, that is, the change in formate geometry, suppression of formyl creation, and diminished decomposition of formic acid, demonstrate that the reaction of formic acid on C–Mo(1 1 0) deviates from that seen on Mo(1 1 0). Dehydration may dominate on Mo(1 1 0), but carbon modification of the surface appears to promote an increased amount of unimolecular deprotonation generating formate and atomic hydrogen at low temperatures. By avoiding the formation of CO and H_2O in the initial decomposition step, the selectivity of the reaction towards desirable products (H_2 and CO_2) should increase. Therefore, the relatively higher proportion of surface formate to formyl suggests that the final products of formic acid decomposition will be impacted by carburization of the surface.

Carburization of the Mo(1 1 0) surface not only changes the amount and mechanism of formate creation, the presence of carbon also increases the stability of formate compared to that on clean Mo(1 1 0). While formate is almost entirely decomposed by 400 K on Mo(1 1 0), C–Mo(1 1 0) stabilizes formate up to at least 500 K as seen by the presence of ν(C–H/D) and ν_s(OCO) in Fig. 2. Notably, Frühberger and Chen observed that the C–Mo(1 1 0) surface dissociates CO at temperatures as low as 500 K; however, the amount of dissociation is dramatically diminished with respect to the clean Mo(1 1 0) surface [57]. Additionally, carburization of Mo(1 1 0) has been shown to increase the selectivity of cyclohexene dehydrogenation [58], and syngas production from CH_3OH [46]. Similarly, in the case of formic acid decomposition, the presence of the carbon on the surface may stabilize formate by withdrawing electrons from the metal surface thereby decreasing the

extent of charge transfer to the formate. Ostensibly, the bonds most affected by charge transfer from the surface to the formate would be those in closest proximity, in this case C–O bonds by which formate is coordinated to the surface. Decreased charge transfer to C–O bonds may cause less destabilization and ultimately a smaller probability of C–O bond cleavage. Alternatively, the change in reactivity may be in part due to site-blocking by carbon atoms. In Mo_2C and C–Mo(1 1 0), carbon atoms reside at the highest coordination surface sites, that is pseudo threefold hollows [4,59]. As stated above, the threefold hollow sites are preferred sites for hydrogen atoms [48], while oxygen atoms are reported to occupy long-bridge sites at low coverages with a transition to threefold hollow sites with increasing oxygen coverage or by co-adsorption with hydrogen [60]. Since carbon resides within or directly below 50% of the threefold hollows on the C–Mo(1 1 0) surface, the presence of carbon could be expected to severely perturb adsorption of species which prefer these sites.

3.2. Temperature programmed desorption of HCOOH

Fig. 3a and b display desorption products following adsorption of 1.6 ML of HCOOH at 77 K onto clean Mo(1 1 0) and C–Mo(1 1 0), respectively. As the sample is heated, the HCOOH multilayer desorbs in a sharp peak at 160 K seen in masses 46, 44, and 28, due to the fragmentation pattern of HCOOH. Molecular desorption of HCOOH from the monolayer continues to ~280 K on both surfaces. On both surfaces, a coincidental peak at 160 K occurs in mass 18 corresponding to H_2O desorption from impurities

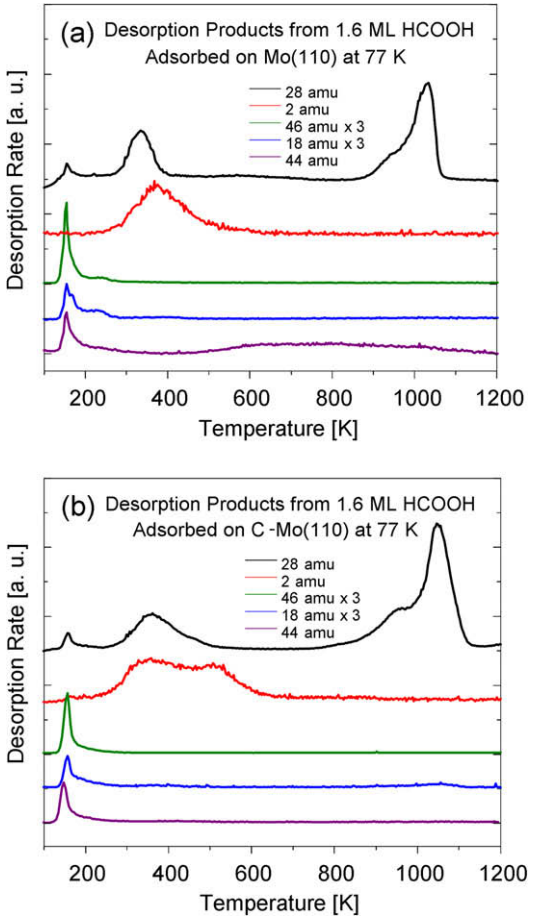

Fig. 3. TPD after adsorption of 1.6 ML HCOOH at 77 K on the (a) Mo(1 1 0) and (b) C–Mo(1 1 0) surfaces. The quadrupole signal has been corrected for the relative sensitivity of each species and masses 46 and 18 were multiplied by three to aid in viewing. The sample linearly heated from 77 to 1200 K at 4 K s^{-1}.

in the HCOOH. Additionally, on Mo(1 1 0) mass 18 displays a small peak at 175 K with a shoulder which extends to ~230 K. Recall that at low temperatures the Mo(1 1 0) surface promotes C–O bond scission to create formyl and hydroxyl groups. Then the mass 18 feature over the range of 175–230 K is attributed to the reaction limited desorption of water formed by the reaction of hydroxyls [42]. The C–Mo(1 1 0) surface shows a much smaller low temperature desorption feature (shown in Supplementary material), since low temperature C–O bond scission is largely suppressed. Hydrogen desorbs from Mo(1 1 0) with a symmetric peak at ~ 375 K, while hydrogen desorbs from C–Mo(1 1 0) as a broad feature with peaks at 350 and 525 K. An increase in the desorption temperature for H_2 from the C–Mo(1 1 0) surface, with respect to the clean Mo(1 1 0) surface, demonstrates greater stability of the formate intermediate on C–Mo(1 1 0) which is in agreement with RAIRS measurements conducted on the two samples (Figs. 1a and 2a). Carbon monoxide evolves from both Mo(1 1 0) and C–Mo(1 1 0) in several distinct features, a low temperature peak, 300–500 K, and two high temperature peaks at 950 and 1050 K. The low temperature CO desorption results from CO created directly from the decomposition of formate and formyl, while both high temperature CO desorption features on Mo(1 1 0) and C–Mo(1 1 0) are attributed to recombinative desorption of atomic carbon and oxygen bound to the surface [35,37,54]. On the initially clean Mo(1 1 0) surface, atomic carbon and oxygen are exclusive products from the complete decomposition of HCOOH on the surface [37]. However, for C–Mo(1 1 0) atomic oxygen from HCOOH also reacts with lattice carbon to evolve CO at high temperatures leading to an overall loss of carbon from the surface. Repeated experiments progressively remove carbon and eventually oxidize the surface. On Mo(1 1 0), temperature programmed desorption of HCOOH leads to residual atomic oxygen on the surface. Unfortunately, the CO and H_2 desorption features from both surfaces are desorption limited, not reaction limited, thus kinetic analysis of the TPD spectra can not provide a measure of the activation energy for formate decomposition on the surface.

Formic acid was adsorbed at 77 K on C–Mo(1 1 0) with coverages ranging from 0.03–1.6 ML. Subsequent temperature programmed desorption spectra m/z^+ 46, 44, 28, 18, and 2 are provided in Supplementary material (Fig. S2a–e). The TPD spectra indicate that the main desorption products observed from the sample are CO, H_2, and HCOOH. Desorption integrals of CO and H_2 increase linearly with increasing HCOOH coverage and plateau for coverages greater than ~0.65 ML. At an HCOOH coverage of ~ 0.16 ML a small H_2O desorption peak can be seen at 360 K which gains intensity with increasing HCOOH coverage up to 0.48 ML. Due to the high desorption temperature, this water must be formed from decomposition of formate. Additionally, a slight peak can be detected at ~200 K due to reaction of hydroxyl groups formed in conjunction with formyl, although this feature is strongly diminished in comparison to clean Mo(1 1 0). The desorption feature for H_2O at 160 K is attributed to H_2O impurities in the HCOOH source. A small desorption feature for CO_2 is evident with a peak located at ~460 K with a shoulder extending to 550 K. However, this feature is very small, due in part to adsorption of CO_2 on the sample mounting probe which is at 77 K. At exposures greater than ~0.3 ML molecular HCOOH is observed to desorb, after which the total HCOOH desorption increases approximately linearly.

On the C–Mo(1 1 0) surface, vibrational spectra and TPD results indicate that the probability of C–O bond dissociation in the initial reaction of formic acid is suppressed by the introduction of carbon. Consequently, this leads to the generation of larger quantities of formate species and significantly less formyl than observed on clean Mo(1 1 0). Upon heating, formate decomposes mostly via C–O bond cleavage generating CO as well as atomic oxygen and hydrogen. A minor reaction pathway produces only small amounts

of CO_2 by deprotonation of formate, presumably due to the continued oxophilic nature of C–Mo(1 1 0). However, hydrogen desorbs largely as H_2 with minimal amounts of H_2O. Xu and Goodman have proposed mechanisms for the temperature programmed reaction of formic acid on clean Mo(1 1 0) [42,61] which are consistent with the TPD and RAIRS data presented here. On Mo(1 1 0) formic acid initially reacts via bimolecular dehydration [$2HCOOH_{ad} \rightarrow H\text{-}CO_{ad} + HCOO_{ad} + H_2O$] or by simple C–O bond scission [$HCOO\text{-}H_{ad} \rightarrow HCO_{ad} + OH_{ad}$] dependent on the surface coverage [42]. All formate species created were observed to decompose by dissociation of the C–O bond producing a mixture of atomic species and CO_{ad}. Formyl was seen to dissociate to atomic hydrogen and CO_{ad} [$HCO_{ad} \rightarrow H_{ad} + CO_{ad}$]. Previously, Madix and co-workers found that carburization of tungsten [62,63] and nickel surfaces [64–66] induced dramatic changes in reactivity towards formic acid. Carbon modification of W(1 0 0) to form W(1 0 0)-(5 × 1)C was observed via TPD and AES experiments to entirely prevent dissociative adsorption of CO [62] and to suppress complete dissociation of formic acid [63]. In contrast to the clean W(1 0 0) surface which completely dissociated formic acid, adsorption of formic acid at 300 K on the W(1 0 0)-(5 × 1)C surface created large amounts of formate which decomposed at 540 K to predominately CO_2 and H_2 with ~5–10% CO and H_2O [63]. Similar results were observed in comparisons of the clean Ni(1 0 0) and carbon-modified Ni(1 0 0)-p(2 × 2)C surfaces [64]. Following exposure to formic acid at 300 K, clean Ni(1 0 0) generated equal amounts of H_2, CO, and CO_2 as well as residual atomic oxygen [22]; however, on the Ni(1 0 0)-p(2 × 2)C surface only H_2 and CO_2 evolved after dosing formic acid [64]. Additionally, carburization of Ni(1 1 0) to form Ni(1 1 0)-(4 × 5)C and Ni(1 1 0)-(2 × 1)C lead to ten times greater selectivity towards the formation of CO_2 and H_2 after exposure to formic acid at 315 K than clean Ni(1 1 0) although the overall activity towards formic acid decomposition decreased by two orders of magnitude [65,66]. Incorporation of carbon on Ni(1 1 0) surfaces was postulated to suppress C–O bond dissociation such that the formyl intermediate was not created leading to enhanced selectivity towards dehydrogenation [66]. Enhanced selectivity of these surfaces was generally attributed to inhibition of formyl production, stabilization of formate intermediates, and the inability of the carbide surfaces to dissociate CO_2.

3.3. Reactive molecular beam scattering of HCOOH and kinetic analysis

To access reactivity information about HCOOH on Mo(1 1 0) and C–Mo(1 1 0), reactive molecular beam scattering (RMBS) experiments were conducted for both surfaces over the 350–700 K temperature range. Fig. 4 illustrates two RMBS experiments which were conducted on the pristine Mo(1 1 0) surface (Fig. 4a) and the C–Mo(1 1 0) surface (Fig. 4b) at a temperature of 600 K. Before the experiment begins, the sample is annealed at 1200 K to desorb any species adsorbed from background (H_2O and CO), and the composition and order of the sample surface is confirmed using RAIRS of CO adsorbed at 77 K, as described in the experimental details. To begin the experiment, the sample is rapidly heated to the desired temperature, in this case 600 K. Once the temperature and background pressure have stabilized, typically less than 1 min, the molecular beam is impinged onto an inert stainless steel flag within the scattering chamber, t = 0–60 s. At t = 60 s, the inert flag is retracted so that the formic acid beam strikes the sample surface. This results in an immediate drop in m/z^+ 46 in the chamber, as a substantial fraction of the formic acid reacts at the sample surface, and simultaneous rises for m/z^+ 28, 2, 18, and 44 indicating production of CO, H_2, H_2O, and CO_2, respectively. The initially high production rate seen for the reaction products gradually decreases within ~45–60 s, dependent on the sample temperature, after which it plateaus and remains nearly constant for reaction times

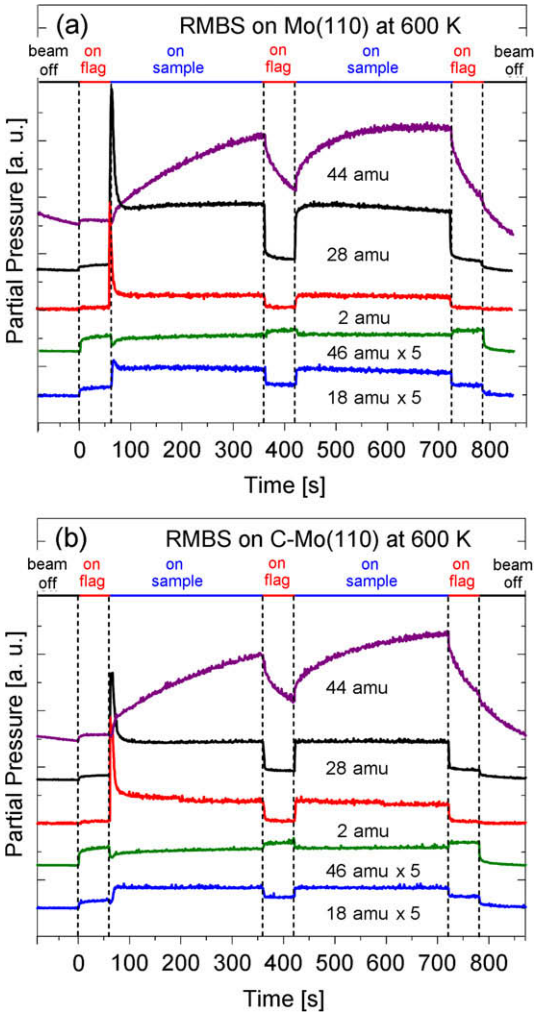

Fig. 4. Reactive molecular beam scattering (RMBS) of HCOOH on (a) the Mo(1 1 0) surface and (b) the C–Mo(1 1 0) surface at 600 K. At t = 0 s, the molecular beam is impinged on the inert flag, and the mass spectra are indicative of HCOOH. At t = 60 s, the flag is removed such that beam strikes the sample surface and reacts to form CO and H_2O by dehydration and CO_2 and H_2 by dehydrogenation. The flag blocks the beam again from t = 360 to 420 s, and again at t = 720–780 s, after which the molecular beam is blocked from entering the scattering chamber.

greater than 10 min. Apparently, the clean surface at the first instant of interaction with the formic acid molecular beam is much more reactive than the surface which is present at steady-state. After impinging formic acid for 300 s on the sample, the inert flag is introduced for another 60 s to aid in distinguishing the relative contributions of the products (CO, H_2, H_2O and CO_2) from the reactant (HCOOH) in the QMS. After re-establishing this baseline, formic acid is impinged again for 300 s onto the sample, followed by 60 s on the inert flag, and then the molecular beam is blocked from entering the scattering chamber. Additional experiments were performed in a similar manner; however, for these experiments the molecular beam was chopped by the inert flag every 60 s for a period of 60 s. This second variant of experiment provided greater certainty for calculating the relative rates of production for the reaction products (CO, CO_2, H_2O, and H_2). It should be noted that the partial pressure of CO_2 in the chamber behaves rather differently than that of the four other gas phase species (HCOOH, CO, H_2O, and H_2). The reason for this is due to slow adsorption and desorption processes on the liquid nitrogen cooled probe in the vacuum chamber. The resulting behavior appears as a slow effective pumping speed for CO_2, in comparison to the other species, and is responsible for a baseline CO_2 pressure which

increases throughout the experiment and a slow exponential decay of the CO_2 pressure after blocking the beam with the inert flag.

The reactive molecular beam scattering experiments provide useful kinetic data, acquired at the first instant of reaction as well as under steady-state conditions. The overall conversion as a function of temperature and time, the product selectivity at steady-state, the steady-state yield of each product, and the activation energy for the dominant reaction pathways can be obtained from these measurements. Using a molecular beam flux of $\sim 1.4 \times 10^{15}$ molecules cm^{-2} s^{-1}, we measured the rate of formic acid consumption from 350 to 700 K on both the Mo(1 1 0) and C–Mo(1 1 0) samples. Over this range, the apparent activation energy for HCOOH decomposition was 20.5 ± 1.9 kJ mol^{-1} and 14.8 ± 1.3 kJ mol^{-1} (data not shown), respectively. The estimated uncertainty is calculated from a statistical analysis of the linear fit. Product selectivity was also calculated for the steady-state conversion of HCOOH. At steady-state, we assume that the accumulation of species on the surface is negligible compared to the overall rate of reaction. By doing so, the relative rates of reaction for the primary reactions can be estimated by measuring the distribution of gas phase products. Only CO, H_2, H_2O, and CO_2 can be detected so we assume that there are only two overall reactions; dehydrogenation ($HCOOH \rightarrow H_2 + CO_2$) and dehydration ($HCOOH \rightarrow H_2O + CO$). Furthermore, the production rate of H_2 is linearly correlated to that of CO_2 while the production rate of H_2O is linearly correlated to that of CO, as shown in Supplementary material (Fig. S3), providing additional evidence that only these two reactions occur. Possible reaction intermediates or individual mechanisms are addressed in discussion later. Therefore, the relative rates of formic acid consumption from dehydrogenation (the desired pathway) or dehydration (the undesired pathway) for both model catalysts can be compared. Due to ease of detection and high signal-to-noise levels within the QMS, we monitor H_2 to determine the rate of dehydrogenation and CO to determine the rate of dehydration. This treatment is justified as the correlation between H_2 and CO_2 production (dehydrogenation) and H_2O and CO production (dehydration) are highly linear, confirming that the two dominant reaction mechanisms are solely dehydration and dehydrogenation. The turn over frequencies for the production of H_2 and CO are plotted in the Supplementary material (Fig. S4). Fig. 5 shows the fraction of HCOOH decomposition which proceeds by dehydrogenation on the Mo(1 1 0) and C–Mo(1 1 0) surfaces as a function of sample temperature.

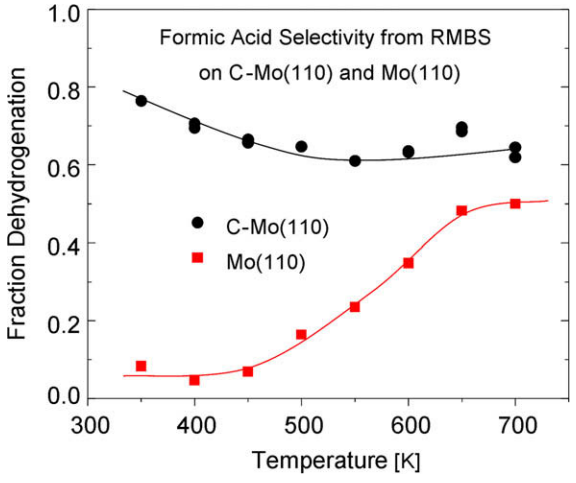

Fig. 5. Fraction of HCOOH consumed which decomposes by dehydrogenation for C–Mo(1 1 0) and clean Mo(1 1 0) as a function of temperature. The flux of HCOOH to the surface was 1.4×10^{15} molecules cm^{-2} s^{-1}.

From Fig. 5 it is clear that the C–Mo(1 1 0) surface is significantly more selective towards the dehydrogenation of HCOOH than the clean Mo(1 1 0) surface at all temperatures investigated (350–700 K). However, it is at lower temperatures 350–450 K where the greatest differences can be seen. Over this temperature range, the C–Mo(1 1 0) sample is ~10–15 times more selective than Mo(1 1 0) for the production of CO_2 and H_2. The C–Mo(1 1 0) selectively dehydrogenates ~70–75% of the formic acid in the 350–450 K range in comparison to Mo(1 1 0) which dehydrogenates ~5%. Notably, the selectivity of C–Mo(1 1 0) compares favorably to that of polycrystalline platinum which dehydrogenated ~85% of incident formic acid in the comparable experiments of Dahlberg et al. [33]. As the surface temperature increases, the selectivity of C–Mo(1 1 0) decreases slightly while the selectivity for Mo(1 1 0) increases dramatically. At a sample temperature of 700 K, the C–Mo(1 1 0) surface is only ~30% more selective than the Mo(1 1 0) surface. Significantly, the products of formic acid decomposition obtained from the steady-state RMBS experiments on both Mo(1 1 0) and C–Mo(1 1 0) differ from those measured by TPD (Fig. 3). These differences may be linked to three separate effects: (1) increased probability of accessing additional reaction pathways during RMBS at elevated temperatures (as opposed to adsorbates undergoing desorption before reaction during TPD), (2) changes in the surface composition as the reaction reaches steady-state (accumulation of atomic oxygen from total decomposition of formic acid), and (3) reactions between adsorbate species or site-blocking by co-adsorbates. The relative rates of the dehydrogenation and dehydration reactions on each surface as a function of temperature are shown in Fig. 6. The individual activation energies for the dehydrogenation ($E_{A,H2}$) and dehydration ($E_{A,H2O}$) reactions on each surface are calculated by analyzing the formation rates of H_2 and CO, respectively, for HCOOH decomposition at sample temperatures ranging from 350 to 700 K. The resulting values provide additional insight into the underpinnings of this effect.

First, $E_{A,H2O}$ is very similar for both surfaces, 16.8 ± 1.5 kJ mol^{-1} for Mo(1 1 0) and 15.6 ± 1.2 kJ mol^{-1} for C–Mo(1 1 0). Clearly, the carbon modification of the surface has little effect on the barriers for the rate-determining step of the dehydration reaction. However, a comparison of the overall rate of dehydration activity on each surface reveals that the C–Mo(1 1 0) surface has a rate of dehydration ~31% ± 7% that of the Mo(1 1 0) at every temperature. This is also reflected in the ratio of the pre-exponential factors for the dehydration reaction where the pre-exponent for dehydration on C–Mo(1 1 0) is one-fourth the value of the pre-exponent on Mo(1 1 0), or $(k_{C-Mo,H2O}/k_{Mo,H2O}) = 0.25$. Hence, the similarities in activation energy suggest that a similar mechanism is responsible for dehydration on both surfaces. Then the difference in rate of dehydration is attributed to a decrease in the concentration of active sites by a factor of approximately four on C–Mo(1 1 0), possibly due to site-blocking by interstitial carbon atoms. Calculated values for $E_{A,H2}$ for each surface are 34.4 ± 3.3 and 12.8 ± 1.0 kJ mol^{-1} for clean Mo(1 1 0) and C–Mo(1 1 0), respectively, representing a decrease of 63% in the activation barrier for dehydrogenation due to the addition of carbon. The pre-exponentials for dehydrogenation on the two surfaces are dramatically different, with a ratio of $(k_{C-Mo,H2}/k_{Mo,H2}) = 0.016$. Thus, due to large differences in both the activation energy and the pre-exponentials for dehydrogenation on the two surfaces, it seems likely that the mechanism for dehydrogenation on C–Mo(1 1 0) is distinct from that on clean Mo(1 1 0).

Vibrational spectra were acquired during RMBS of HCOOH on the Mo(1 1 0) and C–Mo(1 1 0) surfaces. Fig. 7 display spectra acquired at surface temperatures of 400 and 500 K and display several vibrational features for new surface intermediates not

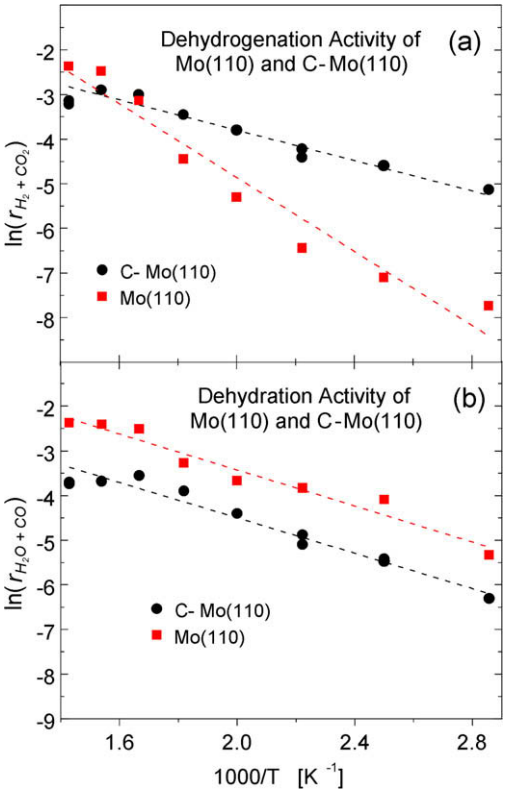

Fig. 6. Arrhenius plots for (a) dehydrogenation and (b) dehydration reactions on the Mo(1 1 0) and C–Mo(1 1 0) surfaces. Carburization of the molybdenum surface leads to a significant decrease in $E_{A,H2}$ from 34.4 ± 3.3 kJ mol^{-1} for Mo(1 1 0) to 12.8 ± 1.0 kJ mol^{-1} for C–Mo(1 1 0). The barrier for dehydration, $E_{A,H2O}$ is only slightly affected by the surface modification with values of 16.8 ± 1.5 kJ mol^{-1} and 15.6 ± 1.2 kJ mol^{-1} for Mo(1 1 0) and C–Mo(1 1 0), respectively. The flux of HCOOH to the surface was 1.4×10^{15} molecules cm^{-2} s^{-1}. Rates for dehydrogenation and dehydration were obtained from the partial pressure of H_2 and CO, respectively.

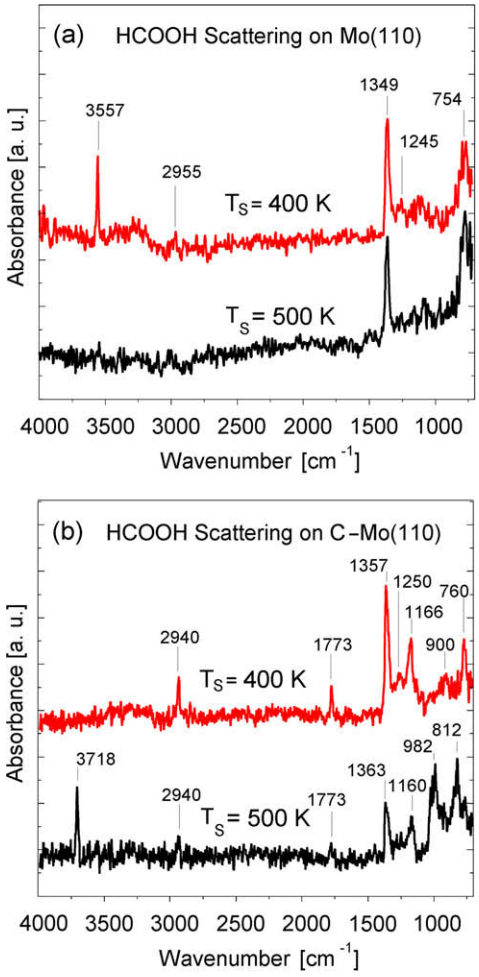

Fig. 7. RAIRS spectra acquired during RMBS experiments on (a) the Mo(1 1 0) surface and (b) the C–Mo(1 1 0) surface at sample temperatures of 400 and 500 K.

observed during experiments conducted by low temperature adsorption and annealing of formic acid. Scattering of HCOOH on Mo(1 1 0) at 400 K (Fig. 7a) results in vibrational peaks at 755, 1349, and 2955 cm^{-1} indicating the presence of bridge-bonded formate. Peaks observed at 3280 and 3557 cm^{-1} are similar to observations made by HREELS on Mo(1 1 0) by other investigators and likely correspond to ν(HOH) of water and ν(OH) of surface hydroxyls, respectively [42,46,67]. Additionally, a weak feature at 1245 cm^{-1} may correspond to a ν_s(OCO) mode due to a small amount of monodentate formate although the ν_a(OCO) feature, expected at ~1740 cm^{-1} [42], is not apparent. If the same experiment is conducted at 500 K, the relative population of bridge-bonded formate is quite similar to the concentration at 400 K; however, the presence of water and hydroxyl groups is greatly diminished. We expect that the greater concentration of hydroxyls present on the surface at 400 K, in comparison to that seen at 500 K, reflect the fact that hydroxyl groups formed via dehydration would recombinatively desorb at higher rates at 500 K resulting in a lower concentration on the Mo(1 1 0) surface. Additionally, a slightly greater percentage of formic acid is dehydrated at 400 K, 95%, than at 500 K, 84%.

Inspection of the RAIRS spectra acquired from C–Mo(1 1 0) at 400 and 500 K (Fig. 7b) reveal significant differences in comparison to the Mo(1 1 0) surface. At 400 K, the C–Mo(1 1 0) surface is partially covered by formate, similar to Mo(1 1 0). On the other hand, both monodentate (760, 1250, 1773 and 2940 cm^{-1}) as well as bridge-bonded formate (760, 1357, and 2940 cm^{-1}) are present. It is unclear in this case; however, the presence of monodentate species may be related to the increased selectivity of C–Mo(1 1 0) towards dehydrogenation. Chen et al. proposed that during electrocatalysis of formic acid on platinum films the bridge-bonded formate species is actually a site-blocker and not an active intermediate [68]. Then perhaps, *monodentate* formate is a precursor for dehydrogenation. Other notable differences include the complete lack of any hydroxyl feature, ν(OH), and the presence of two peaks located at 1166 and 900 cm^{-1}. Xu et al. previously reported similar vibrational features detected by HREELS at 1155 and 855 cm^{-1} corresponding to the ν_s(OCO) and δ(OCO) vibrational modes due to $CO_2^{\delta-}$ formed by HCOOH adsorption on oxygen modified Mo(1 1 0) [42,61]. As shown in the Supplementary material (Fig. S2), formate decomposes to evolve H_2 (350–525 K) and CO_2 (350–550 K) from the C–Mo(1 1 0) surface, and this observation further supports the identification of $CO_2^{\delta-}$ since this species is expected to be the direct precursor to gas phase CO_2. Observable surface concentrations of $CO_2^{\delta-}$ detected via RAIRS during steady-state reaction at 400 K suggest that dehydrogenation of the active formate is facile in comparison to $CO_2^{\delta-}$ desorption from the surface which may limit the overall rate of dehydrogenation. Thus, it appears that decomposition of monodentate formate may be primarily responsible for H_2 and CO_2 production from C–Mo(1 1 0) at 400 K.

Scattering formic acid at 500 K on C–Mo(1 1 0) (Fig. 7b) leads to several changes in the quantity and identity of the surface species. Both monodentate and bridge-bonded formate are still present at 500 K; however, the concentration of both these species is

Table 2
Predicted vibrational frequencies of carboxyl on transition metal surfaces in comparison to experimentally observed features on C–Mo(1 1 0).

Mode	On-top (H up) OCOH/Pt(1 1 1) [69]	On-top OCOH/Pt(2 1 1) [69]	On-top OCOH/Cu(1 1 1) [70]	OCOH on Rh_4 cluster [71]	OCOH on C–Mo(1 1 0) at 500 K
νOH	3670	3706	3637	3701	3718
ν_aOCO	1721	1505	1749	1732	–
ν_sOCO	1225	1166	1106	1104	1160
δOCO	1052	1044	893	–	982

diminished. Additionally, new vibrational features appear at 3718 and 812 cm^{-1} and the peaks previously attributed to $CO_2^{\delta-}$ shift, with δ(OCO) moving from 900 to 982 cm^{-1} and ν_s(OCO) shifting from 1166 to 1160 cm^{-1}. The high frequency feature, 3718 cm^{-1}, is identified as the symmetric stretch of a hydroxyl group, ν(OH). This feature could be associated with ν(OH) of surface hydroxyls, although, Hwu et al. have observed surface hydroxyls on clean C–Mo(1 1 0) at 3620 cm^{-1} [46]. Additionally, we have generated surface hydroxyls by scattering a molecular beam of H_2O on C–Mo(1 1 0) at 200 K leading to a feature at 3617 cm^{-1} (data not shown) in close agreement with Hwu et al. [46]. Since the values for surface hydroxyls are nearly 100 cm^{-1} lower than this new feature, the peak at 3718 cm^{-1} is attributed to a hydroxyl group which is part of a larger surface intermediate, most likely carboxyl (OCOH).

In studies of the water–gas shift reaction on transition metal surfaces, several groups have used density functional theory (DFT) calculations to demonstrate that carboxyl groups represent the most likely active surface intermediates, while formates are spectator species [69–73]. Experimentally, this has proven difficult to confirm. Predicted vibrational frequencies for selected normal modes of the carboxyl intermediate are displayed in Table 2 [69–71], and are compared to the experimentally observed peaks for steady-state HCOOH decomposition on C–Mo(1 1 0) at 500 K. Agreement between the predicted and observed vibrational modes is relatively close. The occurrence of the ν(OH) feature at such high wavenumbers is strong evidence for the presence of a carboxyl species on C–Mo(1 1 0). As we have shown, a value 3718 cm^{-1} is approximately 100 cm^{-1} greater than values for surface hydroxyl groups, but lies very close to values predicted by Mavrikakis and co-workers for carboxyl on Pt [69] and Cu [70] surfaces and Zeinalipour-Yazdi and Efstathiou for carboxyl on four-atom Rh clusters [71]. In the RAIRS spectrum, there is no observable feature which can be uniquely identified as the ν_a(OCO) mode for OCOH, although this may be due to surface selection rules masking the dipole moment. Additionally, the predicted values for ν_a(OCO) are very similar to those for the monodentate formate species seen at 1773 cm^{-1} which could complicate identification. The experimentally observed value for ν_s(OCO) for OCOH varies only slightly, ~6 cm^{-1}, from that seen for $CO_2^{\delta-}$; however, the δ(OCO) normal mode for OCOH is ~80 cm^{-1} greater than that for $CO_2^{\delta-}$. Further, δ(OCO) for OCOH on C–Mo(1 1 0) matches closely with predicted values from DFT calculations. We can not rule out the possibility that a small quantity of the $CO_2^{\delta-}$ species is still present on the C–Mo(1 1 0) surface due to the similarities in the frequency of the ν_s(OCO) mode of both species. However, the additional vibrational losses which are observed support the identification of a carboxyl intermediate on the C–Mo(1 1 0) surface during steady-state formic acid decomposition at 500 K.

The presence of carboxyl may be attributed to two separate reaction mechanisms. First, direct activation of the C–H bond in formic acid may occur upon adsorption onto the C–Mo(1 1 0) surface (HCOOH → H + OCOH). This step would likely be followed by dissociation of the O–H bond leading directly to the formation of a $CO_2^{\delta-}$ surface species and the eventual production of CO_2 and H_2. The activation barrier for the C–H bond would certainly be greater than the barrier for O–H bond dissociation which occurs at temperatures as lows as 215 K, as shown in Fig. 2a. Then, the data suggests a surface temperature of at least 500 K is necessary for the rate of C–H bond activation of formic acid to be great enough to form detectable amounts of carboxyl. Second, the carboxyl species may be formed by the reaction of adsorbed CO and a surface hydroxyl (CO + OH → OCOH), after which O–H bond scission would lead to CO_2 and H_2. It is important to emphasize, that this second mechanism (CO + OH → OCOH) requires the prior formation of CO and OH groups by dehydration. Therefore, this mechanism does not reflect the primary reaction of formic acid, but rather a secondary reaction which is very similar to proposed mechanisms for the water–gas shift reaction [69–73]. Notably, molybdenum carbide (Mo_2C) catalysts are highly active for the water–gas shift reaction [7,8], although DFT calculations indicate that this occurs via a redox mechanism which would not create a carboxyl intermediate [11,74]. Thus, it appears that at 500 K carboxyl can be formed directly from the dissociation of the C–H bond in formic acid following adsorption on the C–Mo(1 1 0) surface which demonstrates a new and unique reaction mechanism for the dissociation of formic acid not observed on the clean Mo(1 1 0) surface.

4. Conclusions

We have studied the decomposition of formic acid on the Mo(1 1 0) and C–Mo(1 1 0) surfaces with vibrational spectroscopy, temperature programmed desorption, and reactive molecular beam scattering. Carburization of the model catalyst had dramatic effects on the reaction pathway and product selectivity. The introduction of carbidic carbon on the Mo(1 1 0) surface was shown to suppress the production of formyl, while increasing the fraction of bridge-bonded formate. During TPD of formic acid, the C–Mo(1 1 0) surface evolved CO and H_2 with only trace quantities of CO_2 and H_2O which is attributed to the oxophilic nature of the surface. However, strikingly different behavior was observed during RMBS experiments conducted on the Mo(1 1 0) and C–Mo(1 1 0) surfaces. During steady-state reaction of formic acid at 350–450 K, the Mo(1 1 0) surface promoted dehydration with ~5% or less of the formic acid undergoing dehydrogenation. In this same temperature range, 70–75% of the formic acid was dehydrogenated. Analysis of the reaction kinetics from 350 to 700 K, indicated that the carburization of the surface poisoned the majority of active sites for dehydration while dramatically decreasing the activation energy for dehydrogenation from 34.4 ± 3.3 to 12.8 ± 1.0 kJ mol^{-1}. Finally, RAIRS spectra obtained during steady-state reaction of formic acid showed the presence of new reaction intermediates on C–Mo(1 1 0) including monodentate formate, a $CO_2^{\delta-}$ species, and a carboxyl intermediate which were absent from Mo(1 1 0). On C–Mo(1 1 0) at 400 K, the monodentate formate and the adsorbed $CO_2^{\delta-}$ species are observed while at 500 K the carboxyl intermediate, OCOH, is also evident. The combination of kinetic and vibrational data indicate that the C–Mo(1 1 0) surface promoted dehydrogenation of formic acid via new reaction pathways not active on Mo(1 1 0). At temperatures up to 400 K on C–Mo(1 1 0) dehydrogenation appears to proceed by formic acid deprotonation

(of the O–H bond) to generate monodentate formate, followed by deprotonation (at the C–H bond) to create $CO_2^{\delta-}$ which shortly desorbs. At 500 K, *an additional* reaction pathway becomes apparent which involves initial activation of the C–H bond to create carboxyl, followed by deprotonation to form $CO_2^{\delta-}$, and finally evolution of gas phase CO_2 and H_2.

Acknowledgments

We acknowledge the Defense Threat Reduction Agency (CBT070005974), the National Science Foundation (CTS-0553243) and the Welch Foundation (F-1436). This material is based upon work supported by, or in part by, the US Army Research Laboratory and the US Army Research Office under contract/Grant No. W911NF-09-1-0130. DWF acknowledges helpful conversations with Dr. Jinlong Gong.

Appendix A. Supplementary material

Supplementary data associated with this article can be found, in the online version, at doi:10.1016/j.jcat.2009.10.012.

References

[1] R.B. Levy, M. Boudart, Science 181 (1973) 547–549.
[2] S.T. Oyama (Ed.), The Chemistry of Transition Metal Carbides and Nitrides, Blackie Academic and Professional, London, 1996.
[3] J.G. Chen, B. Frühberger, J.J. Eng, B.E. Bent, J. Mol. Catal. A 131 (1998) 285–299.
[4] H.H. Hwu, J.G. Chen, Chem. Rev. 105 (2005) 185–212.
[5] S.T. Oyama, Catal. Today 15 (1992) 179–200.
[6] J.G. Chen, Chem. Rev. 96 (1996) 1477–1498.
[7] J. Patt, D.J. Moon, C. Phillips, L. Thompson, Catal. Lett. 65 (2000) 193–195.
[8] E.V. Rebrov, S.A. Kuznetsov, M. De Croon, J.C. Schouten, Catal. Today 125 (2007) 88–96.
[9] D.J. Moon, J.W. Ryu, Catal. Lett. 92 (2004) 17–24.
[10] M. Nagai, K. Matsuda, J. Catal. 238 (2006) 489–496.
[11] P. Liu, J.A. Rodriguez, J. Phys. Chem. B 110 (2006) 19418–19425.
[12] G.B. Haxel, J.B. Hedrick, G.J. Orris, Rare Earth Elements – Critical Resources for High Technology, USGS Fact Sheets, U.S.G. Survey.
[13] Y.W. Rhee, S.Y. Ha, R.I. Masel, J. Power Sources 117 (2003) 35–38.
[14] C. Rice, R.I. Ha, R.I. Masel, P. Waszczuk, A. Wieckowski, T. Barnard, J. Power Sources 111 (2002) 83–89.
[15] C. Rice, S. Ha, R.I. Masel, A. Wieckowski, J. Power Sources 115 (2003) 229–235.
[16] P. Waszczuk, T.M. Barnard, C. Rice, R.I. Masel, A. Wieckowski, Electrochem. Commun. 4 (2002) 599–603.
[17] R. Larsen, S. Ha, J. Zakzeski, R.I. Masel, J. Power Sources 157 (2006) 78–84.
[18] N.M. Markovic, P.N. Ross, Surf. Sci. Rep. 45 (2002) 117–229.
[19] P. Heo, M. Nagao, M. Sano, T. Hibino, J. Electrochem. Soc. 154 (2007) B53–B56.
[20] E.C. Weigert, A.L. Stottlemyer, M.B. Zellner, J.G.G. Chen, J. Phys. Chem. C 111 (2007) 14617–14620.
[21] M.R. Columbia, P.A. Thiel, J. Electroanal. Chem. 369 (1994) 1–14.
[22] J.B. Benziger, R.J. Madix, Surf. Sci. 79 (1979) 394–412.
[23] J.L. Falconer, R.J. Madix, J. Catal. 51 (1978) 47–63.
[24] A. Yamakata, J. Kubota, J.N. Kondo, C. Hirose, K. Domen, F. Wakabayashi, J. Phys. Chem. B 101 (1997) 5177–5181.
[25] W. Erley, D. Sander, J. Vac. Sci. Technol., A 7 (1989) 2238–2244.
[26] Y.K. Sun, W.H. Weinberg, J. Chem. Phys. 94 (1991) 4587–4599.
[27] J.L. Davis, M.A. Barteau, Surf. Sci. 256 (1991) 50–66.
[28] E. Jeroro, J.M. Vohs, Catal. Lett. 130 (2009) 271–277.
[29] F.S. Thomas, R.I. Masel, Surf. Sci. 573 (2004) 169–175.
[30] M.R. Columbia, A.M. Crabtree, P.A. Thiel, J. Am. Chem. Soc. 114 (1992) 1231–1237.
[31] N.R. Avery, Appl. Surf. Sci. 11–2 (1982) 774–783.
[32] N. Kizhakevariam, E.M. Stuve, J. Vac. Sci. Technol., A 8 (1990) 2557–2562.
[33] S.C. Dahlberg, G.A. Fisk, R.R. Rye, J. Catal. 36 (1975) 224–234.
[34] D.W. Flaherty, N.T. Hahn, D. Ferrer, T.R. Engstrom, P.L. Tanaka, C.B. Mullins, J. Phys. Chem. C 113 (2009) 9820–9825.
[35] B. Frühberger, J.G. Chen, Surf. Sci. 342 (1995) 38–46.
[36] B. Frühberger, J.G. Chen, J. Am. Chem. Soc. 118 (1996) 11599–11609.
[37] H.H. Hwu, M.B. Zellner, J.G. Chen, J. Catal. 229 (2005) 30–44.
[38] J. Wang, M. Castonguay, J. Deng, P.H. McBreen, Surf. Sci. 374 (1997) 197–207.
[39] M.L. Colaianni, J.G. Chen, W.H. Weinberg, J.T. Yates, J. Am. Chem. Soc. 114 (1992) 3735–3743.
[40] J.W. He, W.K. Kuhn, D.W. Goodman, Surf. Sci. 262 (1992) 351–358.
[41] Y. Mikawa, J.W. Brasch, R.J. Jakobsen, J. Mol. Spectrosc. 24 (1967) 314–329.
[42] C. Xu, D.W. Goodman, J. Phys. Chem. 100 (1996) 1753–1760.
[43] J.E. Crowell, J.G. Chen, J.T. Yates, J. Chem. Phys. 85 (1986) 3111–3122.
[44] D. Sander, W. Erley, J. Vac. Sci. Technol., A 8 (1990) 3357–3360.
[45] R.B. Barros, A.R. Garcia, L.M. Ilharco, Surf. Sci. 591 (2005) 142–152.
[46] H.H. Hwu, J.G. Chen, Surf. Sci. 536 (2003) 75–87.
[47] F. Zaera, E.B. Kollin, J.L. Gland, Surf. Sci. 166 (1986) L149–L154.
[48] M. Okada, A.P. Baddorf, D.M. Zehner, Surf. Sci. 373 (1997) 145–152.
[49] K.T. Queeney, C.M. Friend, J. Phys. Chem. B 102 (1998) 5178–5181.
[50] A. Bandara, J. Kubota, A. Wada, K. Domen, C. Hirose, J. Phys. Chem. 100 (1996) 14962–14968.
[51] A. Bandara, J. Kubota, A. Wada, K. Domen, C. Hirose, J. Phys. Chem. B 101 (1997) 361–368.
[52] S. Haq, J.G. Love, H.E. Sanders, D.A. King, Surf. Sci. 325 (1995) 230–242.
[53] N.R. Avery, Appl. Surf. Sci. 14 (1983) 149–156.
[54] J.G. Chen, M.L. Colaianni, W.H. Weinberg, J.T. Yates, Chem. Phys. Lett. 177 (1991) 113–117.
[55] A.J. Jaworowski, M. Smedh, M. Borg, A. Sandell, A. Beutler, S.L. Sorensen, E. Lundgren, J.N. Andersen, Surf. Sci. 492 (2001) 185–194.
[56] B.E. Hayden, K. Prince, D.P. Woodruff, A.M. Bradshaw, Phys. Rev. Lett. 51 (1983) 475–478.
[57] B. Frühberger, J.G. Chen, Surf. Sci. 342 (1995) 38–46.
[58] J.G. Chen, B. Frühberger, Surf. Sci. 367 (1996) L102–L110.
[59] H.O. Pierson, Handbook of Refractory Carbides and Nitrides: Properties, Characteristics, Processing and Applications, Noyes Publications, Westwood, NJ, 1996.
[60] J. Kröger, S. Lehwald, H. Ibach, Phys. Rev. B: Condens. Matter 58 (1998) 1578.
[61] C. Xu, D.W. Goodman, J. Am. Chem. Soc. 117 (1995) 12354–12355.
[62] J.B. Benziger, E.I. Ko, R.J. Madix, J. Catal. 54 (1978) 414–425.
[63] J.B. Benziger, E.I. Ko, R.J. Madix, J. Catal. 58 (1979) 149–153.
[64] E.I. Ko, R.J. Madix, Appl. Surf. Sci. 3 (1979) 236–250.
[65] R.J. Madix, J. Falconer, J. McCarty, J. Catal. 31 (1973) 316–318.
[66] J. McCarty, R.J. Madix, J. Catal. 38 (1975) 402–417.
[67] D.A. Chen, C.M. Friend, J. Am. Chem. Soc. 120 (1998) 5017–5023.
[68] Y.X. Chen, M. Heinen, Z. Jusys, R.J. Behm, Langmuir 22 (2006) 10399–10408.
[69] L.C. Grabow, A.A. Gokhale, S.T. Evans, J.A. Dumesic, M. Mavrikakis, J. Phys. Chem. C 112 (2008) 4608–4617.
[70] A.A. Gokhale, J.A. Dumesic, M. Mavrikakis, J. Am. Chem. Soc. 130 (2008) 1402–1414.
[71] C.D. Zeinalipour-Yazdi, A.M. Efstathiou, J. Phys. Chem. C 112 (2008) 19030–19039.
[72] X.Q. Gong, P. Hu, R. Raval, J. Chem. Phys. 119 (2003) 6324–6334.
[73] R.A. Ojifinni, N.S. Froemming, J. Gong, M. Pan, T.S. Kim, J.M. White, G. Henkelman, C.B. Mullins, J. Am. Chem. Soc. 130 (2008) 6801–6812.
[74] H. Tominaga, M. Nagai, J. Phys. Chem. B 109 (2005) 20415–20423.